On a New Cyclic Symmetry Formulation Accounting for Boundaries Undergoing Nonlinear Forces

Samuel Quaegebeur, Fabrice Thouverez

On a new cyclic symmetry formulation accounting for boundaries undergoing nonlinear forces

Samuel Quaegebeur[1], and Fabrice Thouverez[1]

Abstract

Although cyclic symmetry theory was initially developed for linear structures, the introduction of nonlinear forces on internal nodes of the fundamental sector does not affect the methodology. Nevertheless, the method is ill-suited when nonlinear forces are applied at the cyclic boundary. The purpose of this paper is to provide a complement to this theory and to propose a cyclic symmetry formulation for structures undergoing nonlinear forces at their cyclic boundary. A complete nonlinear cyclic formulation for such systems is derived in this work. The advantages of such an approach lies in the reduction of computational costs using the cyclic symmetry properties.

The methodology is employed to characterize the dynamics of several mechanical systems. First, it is validated on simplified models of a cyclic system. Two nonlinearities are considered: a one-dimensional friction contact interface and a cubic nonlinearity. Both cases exhibit very different dynamics behaviors, yet, the results obtained with the new strategy are shown to be very accurate. Once the approach is validated, it is employed on a industrial finite element model of turbine bladed disk featuring contact interfaces between the blades' shrouds. The capability of the method to handle large systems is thus demonstrated. For all cases, periodic excitation are applied following either a traveling or standing wave shape for different engines orders.

Keywords

Nonlinear vibrations, Contact nonlinearities, Geomretic nonlinearities, Cyclic symmetry, Harmonic balance method, Shrouded blade

1 - École Centrale de Lyon, Laboratoire de Tribologie et Dynamique des Systèmes, UMR CNRS 5513, 36 avenue Guy de Collongue, Écully, 69134, France

1 Introduction

Cyclic structures can be found in many engineering systems: aircraft engines, windmill, nuclear power plant, and so on. Predicting the life expectancy of such structures is of the utmost importance to ensure their robustness. Decreasing the computational cost of the related numerical simulations thus become a main challenge. The cyclic symmetry theory [1, 2] is usually applied: a fundamental sector (which gets repeated N along a revolution axis to form the full system) is defined and appropriate boundaries conditions on the displacement field are applied. This strategy has been widely used for linear systems [3] as well as nonlinear configurations [4, 5]. However, this theory becomes ill-suited for at least two situations: first, when the symmetry of the structure is broken, i.e, the sectors present differences between each other due to wear, manufacture tolerance [6], second, when the displacements at the boundaries no longer verify the cyclic property. This may come from nonlinear forces applied at these specific nodes for instance. The latter case is considered in the herein research.

A typical example of a structure where the cyclic property of the displacement at the boundary is no longer verified would be the case of the shroud in the turbines of aircraft engines. This type of turbine architecture allows to seal properly the aerodynamic vane of the engine as well as to lower the vibrations through friction interactions. Figure 1 represents a part of the turbine where the contact between adjacent shrouds is highlighted. In practice, designers define the fundamental sector as in Figure 2. However, such a finite element model cannot be used with the cyclic symmetry property because the displacements at the interface of neighboring sectors are not equal. As a consequence, another fundamental sector is created by splitting the mechanical system into two systems and shifting the position of one of them, see Figure 3. In this configuration, the contact area is internal within the fundamental sector and cyclic boundary is now linear. Such a formulation is however unpractical: nodes need to be duplicated and shifted, substructuration techniques [7] become more costly, and in some cases, this approach can not even be applied. The purpose of this paper is to provide an extension to the cyclic symmetry theory where systems with nonlinear cyclic boundaries can be handled (such as the finite element model depicted in Figure 2).

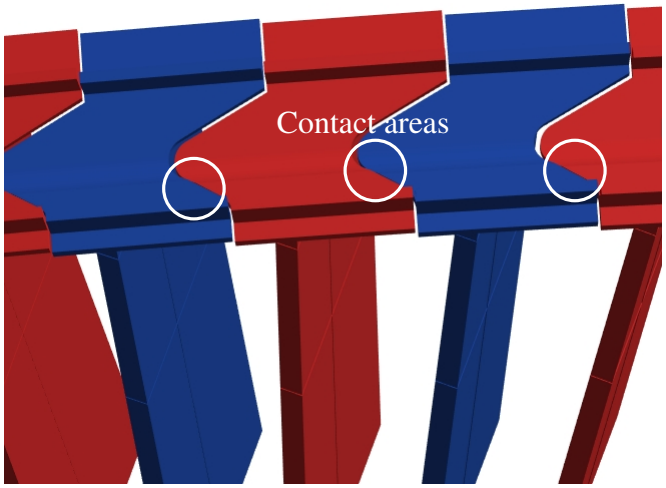

Figure 1. Full system. The blades are identical. Blue and red colors are used for the sake of distinguishing the different sectors

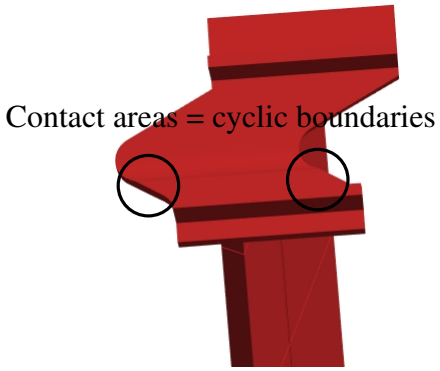

Figure 2. Fundamental sector when the contact area is located at the boundaries.

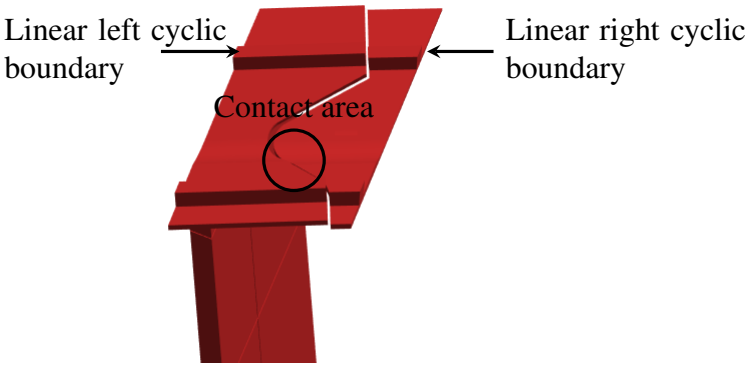

Figure 3. New fundamental sector with linear boundaries.

The study of shrouded bladed disks has been [8, 9] and remains an ongoing research topic [10, 11]. Most papers use the methodology proposed by Siewert et al. [12] to perform numerical investigations. However this strategy, based on Ref [4], imposes a traveling wave excitation on the structure and assumes that the displacement and nonlinear forces are of the same shape. This approach may be pushed to its limits when considering realistic excitations forces, oftentimes more complex. Besides, in a nonlinear context, modal interactions can occur [13] and bifurcated branches can be observed, breaking the traveling wave shape of the solution [14].

The proposed paper proposes a generalization of [12] and is thus not restricted to traveling wave excitations and solutions. Section 2 derives the analytical formulation of the cyclic symmetry when nonlinear forces are applied to the boundary. Section 3 proposes a numerical methodology to seek periodic nonlinear responses and thus gives a reduced form of the general formulation. Finally, Sections 4 and 5 provide numerical demonstration on the proposed method. Spring mass systems, for which a reference solution (computation of the full system solution) is evaluated, are initially employed to validate the approach. A finite element model is then used to show the applicability of the proposed approach to complex structures.

2 Cyclic symmetry formulation

The traditional framework of cyclic symmetry is briefly recalled before being extended to the case of nonlinear boundaries.

2.1 Linear theory

A general linear cyclic system is first considered and is depicted in Figure 4. This system is obtained by the assembly of N fundamental sectors which have been rotated along their revolution axis by an angle equal to $j\alpha = \frac{2\pi j}{N}$ where

j is the number of the sector considered.

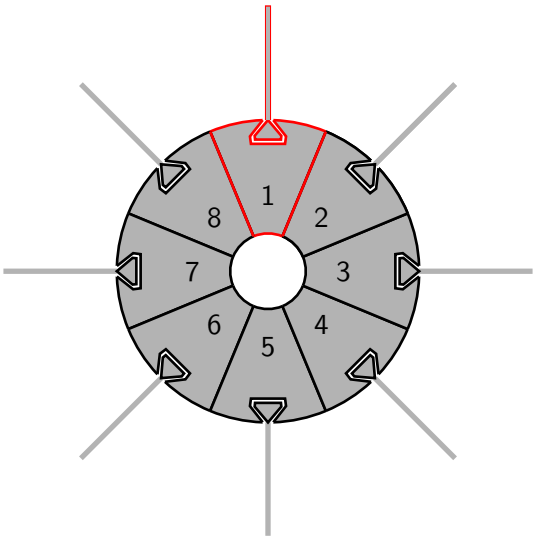

Figure 4. Full cyclic system with $N = 8$. The fundamental sector is highlighted in red.

The equation of motion of an arbitrary sector j reads

$$\mathbf{M}_0\ddot{\mathbf{u}}_j + \mathbf{C}_0\dot{\mathbf{u}}_j + \mathbf{K}_0\mathbf{u}_j + \mathbf{f}_c = \mathbf{f}_{\text{ext},j}, \tag{1}$$

where $\mathbf{M}_0$, $\mathbf{C}_0$, and $\mathbf{K}_0$ denote the mass, damping, and stiffness matrices of the fundamental sector. The vectors $\mathbf{u}_j$ and $\mathbf{f}_{\text{ext},j}$ correspond to the displacement and external forces vectors of sector j. Neighboring sectors, i.e., sectors $j-1$ and $j+1$, apply forces to sector j denoted $\mathbf{f}_{(j-1)\to j}$ and $\mathbf{f}_{(j+1)\to j}$ respectively. These two forces are gathered in $\mathbf{f}_c$. The displacement $\mathbf{u}_j$ is split into three parts: the internal, $\mathbf{u}_{j,\text{i}}$, the left $\mathbf{u}_{j,\text{l}}$, and the right boundaries $\mathbf{u}_{j,\text{r}}$ displacements.

The cyclic symmetry theory consists into two mathematical operations. Both are briefly recalled here, but full details can be found in [1]. First, a change of variables is performed and the physical displacement $\mathbf{u}$ is transformed into a cyclic one, $\tilde{\mathbf{u}}$ through

$$\mathbf{u}_j = \frac{1}{\sqrt{N}} \sum_{k=0}^{N-1} \tilde{\mathbf{u}}_k \mathrm{e}^{\mathrm{i}k(j-1)\alpha}, \forall j \in [\![1, N]\!]. \tag{2}$$

The index k denote the nodal diameter of the system. Since $\mathbf{u}_j$ is a real quantity, $\tilde{\mathbf{u}}_k$ must satisfy

$$\tilde{\mathbf{u}}_k = \tilde{\mathbf{u}}_{N-k}, \forall k \in [\![1, N-1]\!]. \tag{3}$$

As a consequence, knowing the spectral displacement $\tilde{\mathbf{u}}_k$ for $k \in [\![0, K]\!]$, where $K = \frac{N}{2}$ if N is even and $K = \frac{N-1}{2}$ if N is uneven, is sufficient to describe the physical displacement of all sectors.

The second mathematical operation of the cyclic symmetry theory is to formulate the assembly equations in the cyclic domain. Figure 5 shows, in the physical domain, the assembly process for sector j. The equations are

$$\mathbf{u}_{j,\text{r}} = \mathbf{u}_{j+1,\text{l}}, \forall j \in [\![1, N]\!], \text{ with, } \mathbf{u}_{N+1} = \mathbf{u}_1. \tag{4}$$

In the spectral domain [2], it reads

$$\tilde{\mathbf{u}}_{k,\text{r}} = \mathrm{e}^{\mathrm{i}k\alpha}\tilde{\mathbf{u}}_{k,\text{l}}. \tag{5}$$

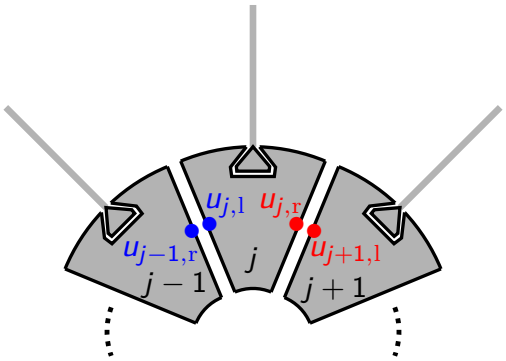

Figure 5. Close-up of the assembly on the boundaries.

Applying these two operations to the equation of motion of a sector (see Equation Eq. (1)) gives, for each nodal diameter k,

$$\tilde{\mathbf{M}}_k\ddot{\tilde{\mathbf{u}}}_k + \tilde{\mathbf{C}}_k\dot{\tilde{\mathbf{u}}}_k + \tilde{\mathbf{K}}_k\tilde{\mathbf{u}}_k = \tilde{\mathbf{f}}_{\mathrm{ext},k}. \tag{6}$$

The matrices $\tilde{\mathbf{M}}_k$, $\tilde{\mathbf{C}}_k$, and $\tilde{\mathbf{K}}_k$ denote the mass, damping, and stiffness matrices for the nodal diameter k. The vector $\tilde{\mathbf{f}}_{\mathrm{ext},k}$ corresponds to the projection of the external forces on the $k-$th nodal diameter. The term $\mathbf{f}_c$ gets canceled during the operation of assembly (third Newton's law). To simplify the proposed theory, only nonlinearities located at the cyclic boundary are considered. Nonlinearities on the internal degrees are handled were already handled in the literature [5, 15].

2.2 New cyclic theory for nonlinear boundaries

A system similar to Figure 1 is considered whose fundamental sector is defined in Figure 2. The equation of motion of such a sector reads

$$\mathbf{M}_0\ddot{\mathbf{u}}_j + \mathbf{C}_0\dot{\mathbf{u}}_j + \mathbf{K}_0\mathbf{u}_j + \mathbf{f}_{\mathrm{nl}} = \mathbf{f}_{\mathrm{ext},j}. \tag{7}$$

The main difference between Equations Eq. (7) and Eq. (1) lies in the interface area and hence in the forces that the neighboring sectors apply to sector j. In the present case, the displacements of neighboring sectors at the interface are different and can not be assembled. The nonlinear forces thus depend on the relative displacement at the interface. The vectors $\mathbf{f}_{\mathrm{nl}}$ contains both the nonlinear forces applied to the right $\mathbf{f}_{\mathrm{nl,r}}$ and left, $\mathbf{f}_{\mathrm{nl,l}}$ boundaries.

Expanding Equation Eq. (7) with a Kronecker product to account for all sectors and applying the changes of variables Eq. (2) lead to, for a nodal diameter k,

$$\mathbf{M}_0\ddot{\tilde{\mathbf{u}}}_k + \mathbf{C}_0\dot{\tilde{\mathbf{u}}}_k + \mathbf{K}_0\tilde{\mathbf{u}}_k + \tilde{\mathbf{f}}_{\mathrm{nl},k} = \tilde{\mathbf{f}}_{\mathrm{ext},j}. \tag{8}$$

The spectral nonlinear forces are obtained with

$$\tilde{\mathbf{f}}_{\mathrm{nl},k} = \frac{1}{\sqrt{N}}\sum_{j=1}^{N}\mathbf{f}_{\mathrm{nl},j}\mathrm{e}^{-\mathrm{i}k(j-1)\alpha}. \tag{9}$$

The physical nonlinear forces can be retrieved with

$$\mathbf{f}_{\mathrm{nl},j} = \frac{1}{\sqrt{N}}\sum_{k=0}^{N-1}\tilde{\mathbf{f}}_{\mathrm{nl},k}\mathrm{e}^{\mathrm{i}k(j-1)\alpha}. \tag{10}$$

The assembly operation of the cyclic symmetry theory (see Equation Eq. (5)) no longer holds because the boundary is nonlinear and the relative displacement is no longer equal to 0. This strategy is here adjusted. Figure 6

depicts the relation between the nonlinear forces of neighboring sectors. The sector $j+1$ applies to sector j a force to its right boundary also written $\mathbf{f}_{\mathrm{nl,r},j}$. Due to Newton's third law the sector j applies the same force to the sector $j+1$ opposite in direction, $\mathbf{f}_{\mathrm{nl,r},j+1}$.

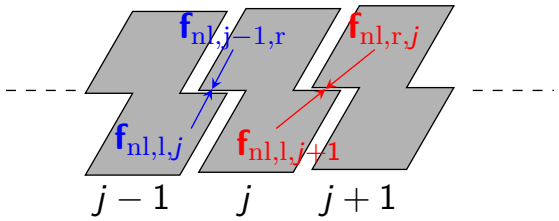

Figure 6. Close-up on the nonlinear boundaries for a configuration involving shrouded blades.

Equation Eq. (4) is thus changed into

$$\mathbf{f}_{\mathrm{nl,r},j} = -\mathbf{f}_{\mathrm{nl,l},j+1}, \forall j \in [\![1, N]\!], \text{ with, } \mathbf{f}_{\mathrm{nl},N+1} = \mathbf{f}_{\mathrm{nl},1}. \tag{11}$$

Substituting Equation Eq. (10) into Eq. (11) gives

$$\frac{1}{\sqrt{N}} \sum_{k=0}^{N-1} \left(\tilde{\mathbf{f}}_{\mathrm{nl,r},k} \mathrm{e}^{\mathrm{i}k(j-1)\alpha} + \tilde{\mathbf{f}}_{\mathrm{nl,l},k} \mathrm{e}^{\mathrm{i}kj\alpha} \right) = \mathbf{0}, \forall j \in [\![1, N]\!] \tag{12}$$

which is equivalent to

$$\sum_{k=0}^{N-1} \left[\mathrm{e}^{\mathrm{i}k(j-1)\alpha} \left(\tilde{\mathbf{f}}_{\mathrm{nl,r},k} + \tilde{\mathbf{f}}_{\mathrm{nl,l},k} \mathrm{e}^{\mathrm{i}k\alpha} \right) \right] = \mathbf{0}, \forall j \in [\![1, N]\!]. \tag{13}$$

This system of equations can be written under the matrix form $\mathbf{A}\mathbf{x} = \mathbf{0}$, where $A_{jk} = \mathrm{e}^{\mathrm{i}k(j-1)\alpha}$ and $x_k = \tilde{f}_{\mathrm{nl,r},k} + \tilde{f}_{\mathrm{nl,l},k} \mathrm{e}^{\mathrm{i}k\alpha}$. Since the determinant of $\mathbf{A}$ is different of zero, a unique solution exists and is $\mathbf{x} = \mathbf{0}$. As a consequence for nonlinear boundaries, Equation Eq. (5) becomes for each nodal diameter k,

$$\tilde{\mathbf{f}}_{\mathrm{nl,r},k} = -\mathrm{e}^{\mathrm{i}k\alpha} \tilde{\mathbf{f}}_{\mathrm{nl,l},k}. \tag{14}$$

For more readability, Equation Eq. (8) is split and reorganized into the internal, right and left boundaries degrees of freedom. Applying Equation Eq. (14) into the resulting system gives

$$\mathbf{M}_{0,\mathrm{new}} \begin{bmatrix} \ddot{\tilde{\mathbf{u}}}_{\mathrm{i},k} \\ \ddot{\tilde{\mathbf{u}}}_{\mathrm{r},k} \\ \ddot{\tilde{\mathbf{u}}}_{\mathrm{l},k} \end{bmatrix} + \mathbf{C}_{0,\mathrm{new}} \begin{bmatrix} \dot{\tilde{\mathbf{u}}}_{\mathrm{i},k} \\ \dot{\tilde{\mathbf{u}}}_{\mathrm{r},k} \\ \dot{\tilde{\mathbf{u}}}_{\mathrm{l},k} \end{bmatrix} + \mathbf{K}_{0,\mathrm{new}} \begin{bmatrix} \tilde{\mathbf{u}}_{\mathrm{i},k} \\ \tilde{\mathbf{u}}_{\mathrm{r},k} \\ \tilde{\mathbf{u}}_{\mathrm{l},k} \end{bmatrix} + \begin{bmatrix} \mathbf{0} \\ -\mathbf{I}\mathrm{e}^{\mathrm{i}k\alpha} \\ \mathbf{I} \end{bmatrix} \tilde{\mathbf{f}}_{\mathrm{nl,l},k} = \begin{bmatrix} \tilde{\mathbf{f}}_{\mathrm{ext,i},k} \\ \tilde{\mathbf{f}}_{\mathrm{ext,r},k} \\ \tilde{\mathbf{f}}_{\mathrm{ext,l},k} \end{bmatrix}, \tag{15}$$

where the matrix $\mathbf{M}_{0,\mathrm{new}}$ is reorganized into

$$\mathbf{M}_{0,\mathrm{new}} = \begin{bmatrix} \mathbf{M}_{0,\mathrm{ii}} & \mathbf{M}_{0,\mathrm{ir}} & \mathbf{M}_{0,\mathrm{il}} \\ \mathbf{M}_{0,\mathrm{ri}} & \mathbf{M}_{0,\mathrm{rr}} & \mathbf{M}_{0,\mathrm{rl}} \\ \mathbf{M}_{0,\mathrm{li}} & \mathbf{M}_{0,\mathrm{lr}} & \mathbf{M}_{0,\mathrm{ll}} \end{bmatrix} \tag{16}$$

and similarly for $\mathbf{K}_{0,\mathrm{new}}$ and $\mathbf{C}_{0,\mathrm{new}}$. The matrix $\mathbf{I}$ is the identity matrix of size the number of nonlinear degrees of freedom on the right boundary. For better readability, the assumption that no nonlinear forces exist at the internal nodes was made. Equation Eq. (15) is most general and enables to treat cyclic symmetric problem when the nonlinearities are located at the boundary (taking into account additional nonlinearities on the internal nodes also works with the proposed approach). In the next section, the formulation is simplified by seeking seeking a solution as a relative periodic displacement.

3 Simplifications by seeking a relative periodic motion

Excitations forces are periodic, hence the solutions of the problem are assumed to be periodic as well. The Harmonic Balance Method (HBM) [16] provides an appropriate framework for such problems and will be used in the following. The spectral displacement is written as a Fourier series with an order of expansion N_h,

$$\tilde{\mathbf{u}}_k = \tilde{\mathbf{c}}_0 + \sum_{n=1}^{N_h} \left(\tilde{\mathbf{c}}_{-n} \mathrm{e}^{-\mathrm{i}n\omega t} + \tilde{\mathbf{c}}_n \mathrm{e}^{\mathrm{i}n\omega t} \right), \tag{17}$$

where $(\tilde{\mathbf{c}}_n)_{n\in[\![-N_h,N_h]\!]}$ are the complex harmonic coefficients. The negative indices correspond to forward traveling components whereas positive indices denote the backward components. In the case $k = 0$ or $k = \frac{N}{2}$, the nodal diameters are non-degenerated [17] and the equality $\tilde{\mathbf{c}}_{-n} = \bar{\tilde{\mathbf{c}}}_n$ must be satisfied. Equation Eq. (17) is then substituted into Eq. (15) and the residual is projected along the basis $\left(\mathrm{e}^{\mathrm{i}n\omega t}\right)_{n\in[\![-N_h,N_h]\!]}$. For an arbitrary harmonic n and an arbitrary nodal diameter k, it gives

$$\begin{bmatrix} \mathbf{Z}_{n,\mathrm{ii}} & \mathbf{Z}_{n,\mathrm{ir}} & \mathbf{Z}_{n,\mathrm{il}} \\ \mathbf{Z}_{n,\mathrm{ri}} & \mathbf{Z}_{n,\mathrm{rr}} & \mathbf{Z}_{n,\mathrm{rl}} \\ \mathbf{Z}_{n,\mathrm{li}} & \mathbf{Z}_{n,\mathrm{lr}} & \mathbf{Z}_{n,\mathrm{ll}} \end{bmatrix} \begin{bmatrix} \tilde{\mathbf{c}}_{\mathrm{i},k,n} \\ \tilde{\mathbf{c}}_{\mathrm{r},k,n} \\ \tilde{\mathbf{c}}_{\mathrm{l},k,n} \end{bmatrix} + \begin{bmatrix} \mathbf{0} \\ -\mathbf{I}\mathrm{e}^{\mathrm{i}k\alpha} \\ \mathbf{I} \end{bmatrix} \langle \tilde{\mathbf{f}}_{\mathrm{nl},\mathrm{l},k}, \mathrm{e}^{\mathrm{i}n\omega t} \rangle = \begin{bmatrix} \mathbf{c}_{\mathrm{ext},\mathrm{i},k,n} \\ \mathbf{c}_{\mathrm{ext},\mathrm{r},k,n} \\ \mathbf{c}_{\mathrm{ext},\mathrm{l},k,n} \end{bmatrix}. \tag{18}$$

The dynamic stiffness matrix $\mathbf{Z}_n$ is equal to $\left(-(n\omega)^2 \mathbf{M}_0 + \mathrm{i}n\omega \mathbf{C}_0 + \mathbf{K}_0 \right)$. The vectors $\mathbf{c}_{\mathrm{ext},k,n}$ denote the harmonic coefficient n of the $k-$th spectral excitation forces and are non-zero only for $n = \pm 1$.

The nonlinearity is located at the boundary and thus depends on the relative motion of the interface. To further reduce the system Eq. (18), two condensations strategies are applied [18]. First, as the internal nodes are linear, they can be expressed as a function of the others nonlinear nodes

$$\tilde{\mathbf{c}}_{\mathrm{i},k,n} = \mathbf{Z}_{n,\mathrm{ii}}^{-1} \left(\mathbf{c}_{\mathrm{ext},\mathrm{i},k,n} - \mathbf{Z}_{n,\mathrm{ir}} \tilde{\mathbf{c}}_{\mathrm{r},k,n} - \mathbf{Z}_{n,\mathrm{il}} \tilde{\mathbf{c}}_{\mathrm{l},k,n} \right). \tag{19}$$

Substituting this equation into the second and third line of Eq. (18) gives

$$\begin{bmatrix} \mathbf{Z}_{n,\mathrm{red},\mathrm{rr}} & \mathbf{Z}_{n,\mathrm{red},\mathrm{rl}} \\ \mathbf{Z}_{n,\mathrm{red},\mathrm{lr}} & \mathbf{Z}_{n,\mathrm{red},\mathrm{ll}} \end{bmatrix} \begin{bmatrix} \tilde{\mathbf{c}}_{\mathrm{r},k,n} \\ \tilde{\mathbf{c}}_{\mathrm{l},k,n} \end{bmatrix} + \begin{bmatrix} -\mathbf{I}\mathrm{e}^{\mathrm{i}k\alpha} \\ \mathbf{I} \end{bmatrix} \langle \tilde{\mathbf{f}}_{\mathrm{nl},\mathrm{l},k}, \mathrm{e}^{\mathrm{i}n\omega t} \rangle = \begin{bmatrix} \mathbf{c}_{\mathrm{ext},\mathrm{red},\mathrm{r},k,n} \\ \mathbf{c}_{\mathrm{ext},\mathrm{red},\mathrm{l},k,n} \end{bmatrix}, \tag{20}$$

where $\mathbf{Z}_{n,\mathrm{red},\mathrm{rr}} = \mathbf{Z}_{n,\mathrm{rr}} - \mathbf{Z}_{n,\mathrm{ri}} \mathbf{Z}_{n,\mathrm{ii}}^{-1} \mathbf{Z}_{n,\mathrm{ir}}$ and similarly for the other reduced dynamic stiffness matrices. The vector $\mathbf{c}_{\mathrm{ext},\mathrm{red},\mathrm{r},k,n}$ is equal to $\left(\mathbf{c}_{\mathrm{ext},\mathrm{r},k,n} - \mathbf{Z}_{n,\mathrm{ri}} \mathbf{Z}_{n,\mathrm{ii}}^{-1} \mathbf{c}_{\mathrm{ext},\mathrm{i},k,n} \right)$. Second, to reduce further the system, a last condensation on the relative displacement is performed. The spectral harmonic nonlinear coefficients are equal to

$$\begin{bmatrix} \tilde{\mathbf{c}}_{\mathrm{r},k,n} \\ \tilde{\mathbf{c}}_{\mathrm{l},k,n} \end{bmatrix} = \begin{bmatrix} \mathbf{Z}_{n,\mathrm{red},\mathrm{rr}} & \mathbf{Z}_{n,\mathrm{red},\mathrm{rl}} \\ \mathbf{Z}_{n,\mathrm{red},\mathrm{lr}} & \mathbf{Z}_{n,\mathrm{red},\mathrm{ll}} \end{bmatrix}^{-1} \left(\begin{bmatrix} \mathbf{c}_{\mathrm{ext},\mathrm{red},\mathrm{r},k,n} \\ \mathbf{c}_{\mathrm{ext},\mathrm{red},\mathrm{l},k,n} \end{bmatrix} - \begin{bmatrix} -\mathbf{I}\mathrm{e}^{\mathrm{i}k\alpha} \\ \mathbf{I} \end{bmatrix} \langle \tilde{\mathbf{f}}_{\mathrm{nl},\mathrm{l},k}, \mathrm{e}^{\mathrm{i}n\omega t} \rangle \right). \tag{21}$$

Its relative motion is obtained with

$$\tilde{\mathbf{c}}_{\mathrm{rel},k,n} = -\mathrm{e}^{-\mathrm{i}k\alpha} \tilde{\mathbf{c}}_{\mathrm{r},k,n} + \tilde{\mathbf{c}}_{\mathrm{l},k,n}. \tag{22}$$

If the relative spectral displacement is equal to 0, i.e. the nodes are at co-located, then Equation Eq. (5) is retrieved. Projecting Equation Eq. (21) on $\left[-\mathbf{I}\mathrm{e}^{-\mathrm{i}k\alpha} \, \mathbf{I} \right]$ gives

$$\mathbf{Z}_{\mathrm{rel},k,n} \tilde{\mathbf{c}}_{\mathrm{rel},k,n} + \langle \tilde{\mathbf{f}}_{\mathrm{nl},\mathrm{l},k}, \mathrm{e}^{\mathrm{i}n\omega t} \rangle = \mathbf{c}_{\mathrm{ext},\mathrm{rel},k,n}, \tag{23}$$

where

$$\mathbf{Z}_{\mathrm{rel},k,n} = \left(\begin{bmatrix} -\mathbf{I}\mathrm{e}^{-\mathrm{i}k\alpha} & \mathbf{I} \end{bmatrix} \begin{bmatrix} \mathbf{Z}_{n,\mathrm{red,rr}} & \mathbf{Z}_{n,\mathrm{red,rl}} \\ \mathbf{Z}_{n,\mathrm{red,lr}} & \mathbf{Z}_{n,\mathrm{red,ll}} \end{bmatrix}^{-1} \begin{bmatrix} -\mathbf{I}\mathrm{e}^{\mathrm{i}k\alpha} \\ \mathbf{I} \end{bmatrix} \right)^{-1} \tag{24}$$

and

$$\mathbf{c}_{\mathrm{ext,rel},k,n} = \mathbf{Z}_{\mathrm{rel},k,n} \begin{bmatrix} -\mathbf{I}\mathrm{e}^{-\mathrm{i}k\alpha} & \mathbf{I} \end{bmatrix} \begin{bmatrix} \mathbf{Z}_{n,\mathrm{red,rr}} & \mathbf{Z}_{n,\mathrm{red,rl}} \\ \mathbf{Z}_{n,\mathrm{red,lr}} & \mathbf{Z}_{n,\mathrm{red,ll}} \end{bmatrix}^{-1} \begin{bmatrix} \mathbf{c}_{\mathrm{ext,red,r},k,n} \\ \mathbf{c}_{\mathrm{ext,red,l},k,n} \end{bmatrix} \tag{25}$$

This equation was obtained for an arbitrary nodal diameter k and harmonic n. However, in practice, an entire set of nodal diameters and harmonics must be taken into account. In order to remain in a most general framework, the methodology developed in [5] is employed: based on the nature of the nonlinearity, the interacting nodal diameters are evaluated and kept in the basis. The evaluation of the term $\langle \tilde{\mathbf{f}}_{\mathrm{nl},l,k}, \mathrm{e}^{\mathrm{i}n\omega t} \rangle$ is decomposed into two parts: a transformation into the physical domain [5] followed by an AFT procedure [19].

The most advantageous part of Equation Eq. (23) is that it does not make any assumption and is very general.

4 Validation on a cyclic symmetric model

4.1 Mechanical model

In this section, two simplified models are considered, see Figure 7. The first case, see Figure 7a, is akin to a shrouded blade system. Its fundamental sector consists of five masses. The sectors of the system are connected to each other by nonlinear forces, modeling a friction contact interface. The Coulomb law is considered

$$\begin{cases} \|\mathbf{f}_{\mathrm{nl,T}}\| & < & \mu \left|\mathbf{f}_{\mathrm{nl,N}}\right| & \text{if } \dot{\mathbf{x}}_{\mathrm{rel,T}} = 0, \\ \mathbf{f}_{\mathrm{nl,T}} & = & -\mu \left|\mathbf{f}_{\mathrm{nl,N}}\right| \frac{\dot{\mathbf{x}}_{\mathrm{rel,T}}}{|\dot{\mathbf{x}}_{\mathrm{rel,T}}|} & \text{otherwise,} \end{cases} \tag{26}$$

where $\mathbf{f}_{\mathrm{nl,T}}$ and $\mathbf{f}_{\mathrm{nl,N}}$ represents the tangential and normal nonlinear forces at the interface node. For this one-dimensional academic test case, no normal direction is considered and $\mathbf{f}_{\mathrm{nl,N}}$ is set to 10 N. The scalar μ represents the friction coefficient and is set to 0.3. The term $\dot{\mathbf{x}}_{\mathrm{rel,T}}$ denotes the relative velocity at the contact interface node. Regularized [20] and non-regularized [21] formulations have been developed throughout the years. In this paper, the Dynamic Lagrangian Frequency Time (DLFT) procedure is employed [22]. This methodology employs the augmented Lagrangian formulation in the frequency domain and is non-regularized.

For the second system, see Figure 7b, the blades are connected through a polynomial nonlinearity

$$f_{\mathrm{nl}} = k_{\mathrm{nl}} \mathbf{x}_{\mathrm{rel}}^3, \tag{27}$$

where $k_{\mathrm{nl}} = 2 \cdot 10^{10}\,\mathrm{N{\cdot}m^{-3}}$ and $\mathbf{x}_{\mathrm{rel}}$ is the relative displacement between two adjacent sectors. Such nonlinearity could model lubrication law for instance. All the parameters of the two models are provided in Table 1. For both cases, $N = 24$ sectors were considered.

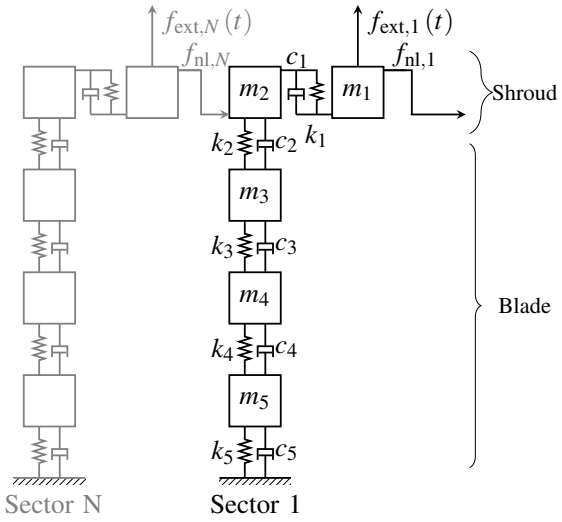

(a) Frictional case

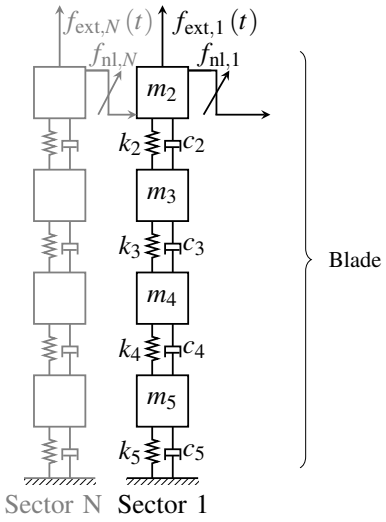

(b) Geometric case.

Figure 7. Representation of two neighboring sectors of the test case. The black sector represents the fundamental sector.

Index	m (in kg)	k(in N·m^{-1})	c(in N·s·m^{-1})
1	0.2	$5 \cdot 10^5$	0.7
2	0.2	$2 \cdot 10^6$	1.3
3	0.3	$1 \cdot 10^6$	0.7
4	0.4	$40 \cdot 10^6$	26.7
5	1.2	$6 \cdot 10^5$	0.4

Table 1. Mass, stiffness, and damping values of the mechanical systems.

An excitation force is applied to the first mass of each sector. Traveling and standing waves excitations are considered with an engine order h_{ex}. To validate the approach proposed in Sections 2 and 3, the strategy is

compared to the full system response. The frequency response functions of the first mass of each sector is illustrated. Throughout the paper, the results are normalized with the linear amplitude and the resonant frequency.

The HBM is performed with $N_h = 5$ harmonics and the period is divided into 100 time-steps for the AFT procedure. The continuation procedure is performed with a pseudo arc-length procedure [23].

4.2 Numerical results for the friction case

To verify the validity of the method for different level of nonlinearities, five levels of forcing, i.e. 0.1, 0.2, 0.3, 0.4, and 0.5 N are applied to the structure. Figure 8 depicts the nonlinear frequency response function of the system for the different cases. A traveling wave solution is obtained and thus all sectors exhibit the same amplitude level. The results of the proposed strategy match perfectly with the ones of the reference solution (full system). As expected, as the excitation amplitude increases, so does the damping.

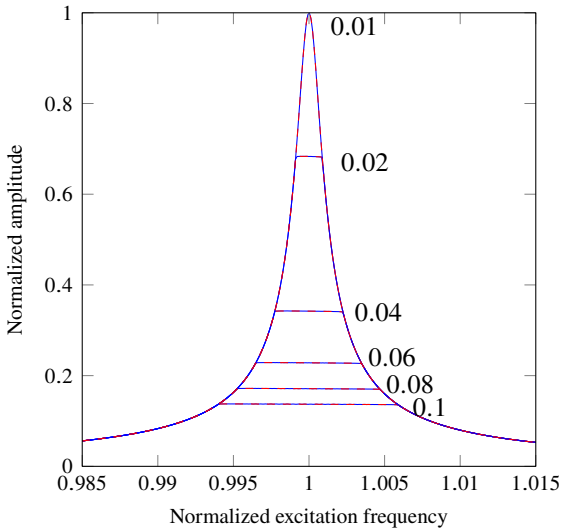

Figure 8. Normalized frequency response function for five levels of forcing for a traveling wave excitation with $h_{ex} = 3$. Reference (——), new method (- -).

Figures 9 and 10 illustrate the nonlinear frequency response function for a standing wave excitation with an amplitude equal to 0.5 N. The Figures show the displacements of the first mass of all sectors. Due to the nature of the excitation, the sectors undergo different level of amplitudes as observed in the Figures 9 and 10. Once again, for both cases, the results match perfectly and thus validate the proposed approach.

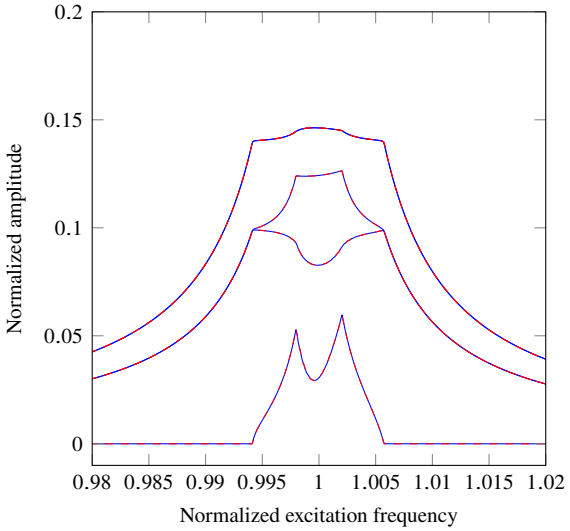

Figure 9. Normalized frequency response function for a standing wave excitation with $h_{ex} = 3$. Reference (—), new method (- -).

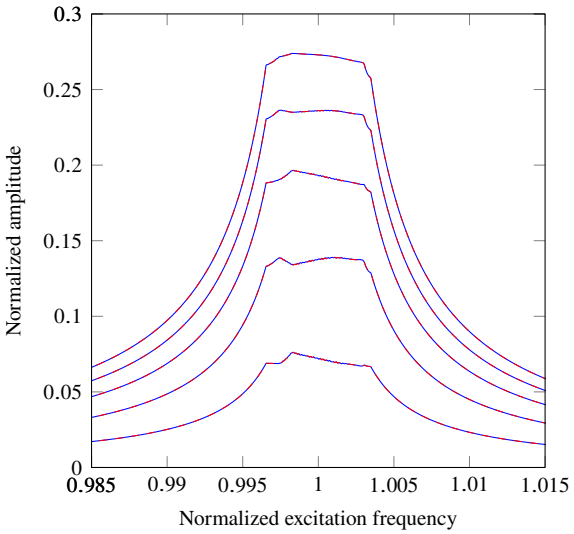

Figure 10. Normalized frequency response function for a standing wave excitation with $h_{ex} = 5$. Reference (—), new method (- -).

Table 2 compares the number of nonlinear unknowns between the methodologies. The reference method considers all the sectors and thus has $N \times (1 + 2N_h)$ nonlinear unknowns. Thanks to the proposed approach, cyclic reduction can be applied [5]. For $h_{ex} = 3$, the third and ninth nodal diameters interact. The associated components are complex hence the system has $2 \times 2 \times (1 + 2N_h)$ real unknowns. Notice that, additionally to this reduction of the number of unknowns, the size of the matrices for the spectral approach are much reduced compared to the ones of the full system.

Methodologies	$h_{ex} = 3$	$h_{ex} = 5$
Reference (full)	264	264
Cyclic	44	132

Table 2. Number of nonlinear unknowns.

4.3 Numerical results for the geometric nonlinearity

The interest of this second test case is two fold. First, there is only one node at the boundary. Therefore, no splitting strategy such as the one exposed in Figure 3 can be applied. Second, a polynomial nonlinearity is considered. Such systems exhibit rich and complex nonlinear behaviour such as bifurcated branches.

A forward traveling wave excitation is first applied to the system with $h_{ex} = 3$ and a level of 1 N. The reduction for this system is similar to the frictional case, see Table 2. Figure 11 illustrates the normalized displacement of the blade tip of the first sector. A hardening behavior (increase of the resonant frequency with respect to the linear case) is observed and is expected from the odd nonlinearity considered (see Equation Eq. (27)). A bifurcated branch was obtained by using the branch switching procedures of Seydel [24] and Kuznetsov [25]. The proposed cyclic symmetry methodology matches perfectly with the reference method.

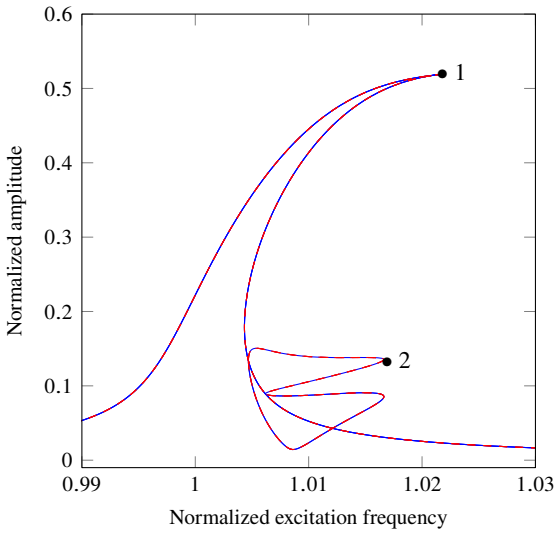

Figure 11. Normalized frequency response function for a traveling wave excitation. (—): reference, (- -): new method. The numbers denote solutions for which the spectral harmonic content will be provided.

Figure 12 and 13 illustrate the harmonic content of each nodal diameter. The forward and backward traveling wave components are distinguished by a negative index for the former and a positive index for the latter. For Figure 12, the main component of the response is the first harmonic of the third nodal diameter. The negative index shows that the main component is a forward traveling wave, similar to the excitation. The other harmonics response (nodal diameter 9 for the third and fifth harmonics) stem from the nonlinearity and traduce a global traveling wave shape of the solution.

The behavior on the bifurcated branch is very different as illustrated in Figure 13. The main component of the response is the first harmonic of the ninth nodal diameter (with a backward wave shape). However the first harmonic of the third nodal diameter also has an high amplitude value. As a consequence the solution does not follow the shape of the excitation and thus strategies such as the ones explained in [4, 12] no longer hold. The proposed methodology however does.

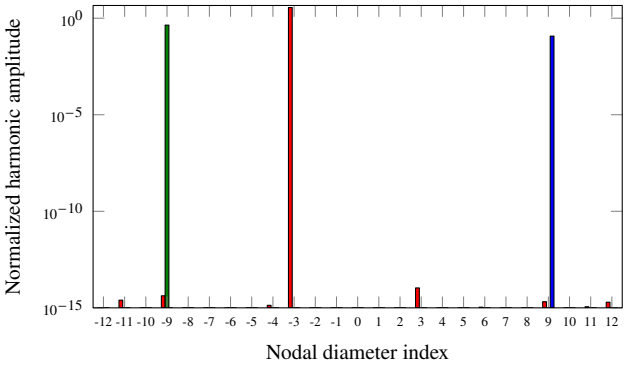

Figure 12. Spectral harmonic content for the solution numbered 1 in Figure 11. (■): first harmonic, (■): third, and (■): fifth harmonics.

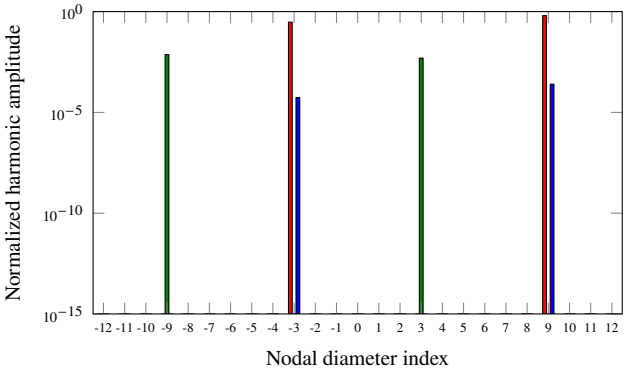

Figure 13. Spectral harmonic content for the solution numbered 2 in Figure 11. (■): first harmonic, (■): third, and (■): fifth harmonics.

A standing wave excitation is now applied to the system with $h_{ex} = 3$. Figure 14 depicts the response of the blade tip of the first sector. The system dynamics is quite complex and multiple bifurcated solution stem from the main branch. The cyclic strategy retrieves perfectly the main branch and one of the bifurcated branches. However the branch number 3 obtained with the reference approach is not retrieved. This observation can be explained in the light of Figure 15 which provides the harmonic content of the nodal diameters of a solution belonging to branch (number) 3. For this solution, nodal diameters 3, 6, 9, and 12 feature a high amplitude and this behavior can not be retrieved with the proposed cyclic method as only nodal diameters 3 and 9 were kept. To retrieve this bifurcated branch a greater cyclic expansion would have been required.

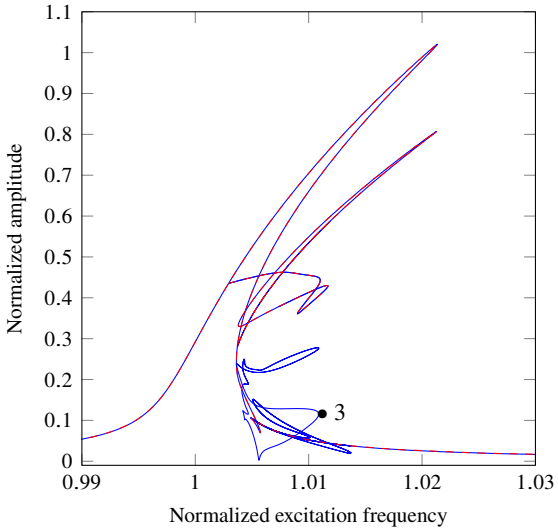

Figure 14. Normalized frequency response function for a standing wave excitation. (—): reference, (- -): new method. The number denotes the solution for which the spectral harmonic content will be provided.

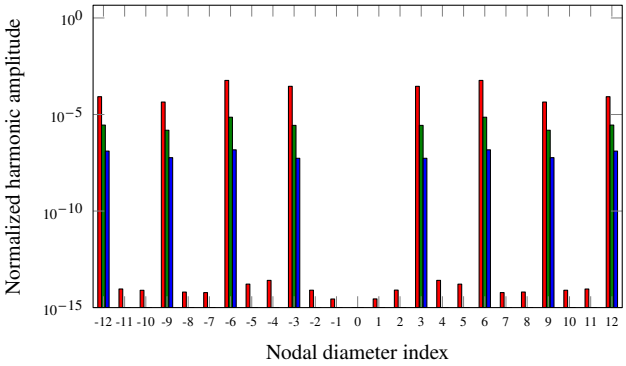

Figure 15. Spectral harmonic content for the solution numbered 3 in Figure 14. (■): first harmonic, (■): third, and (■): fifth harmonics.

5 Application on an industrial case

The proposed strategy is now applied to a realistic shrouded turbine model. For these systems, a rotation matrix is applied to the mechanical system to work on the local reference frame of each node [12]. Moreover a Craig-Bampton reduction [26] is employed to decrease the size of the system. The contact nodes and an excitation node (located at the mid-span of the blades) are kept as master nodes.

5.1 Finite-element model

The finite element model presented in Figure 1 is considered. The structure is composed of 147 sectors, each one is meshed with 3514 nodes, 180 of which are nonlinear, located at the contact areas. The system rotates at 1000 rpm around its revolution axis and a preloading force is considered to account for centrigual effect.

The DLFT is applied to the three-dimensional contact interface and thus the Coulomb's law is completed with

the contact/separation between the bodies. The friction coefficient was taken equal to 0.1

$$\begin{cases} \mathbf{f}_{\mathrm{nl,N}} & \geq & 0 & \text{repulsive force only} \\ \mathbf{x}_{\mathrm{rel,N}} & \geq & 0 & \text{no penetration} \\ \mathbf{x}_{\mathrm{rel,N}} \cdot \mathbf{f}_{\mathrm{nl,N}} & = & 0 & \text{either no force or no contact} \end{cases} . \tag{28}$$

The system is excited at mid-span along the 21$^{\mathrm{st}}$ engine order for both a traveling wave shape or a standing wave. As $h_{ex} = 21$, only nodal diameters 0, 21, 42 and 63 interact. The excitation amplitude is set to 2 N. The excitation frequency is chosen around the first bending mode. The following frequency response functions are illustrated for the excitation point.

5.2 Numerical results

The dynamics of the system is evaluated with the proposed approach: the fundamental sector in Figure 2 is used and the strategy explained in Sections 2 and 3 employed. This method is compared against the traditional approach: i.e. the shroud is split and reassembled to avoid nonlinear interface at the boundary, see Figure 3. Once again, it is important to underline that this remains a modeling trick, that is impractical as it requires a direct intervention of the user to duplicate the boundaries degrees of freedom as well as shift them. Moreover the Craig-Bampton reduction takes a longer time as a greater number of nodes is considered.

The goal of this section is thus to show the robustness of the proposed approach for a more complex system.

The HBM is used with $N_h = 3$ harmonics and 60 time steps. For both approaches, the total number of nonlinear unknowns is equal to $7 \times 180 \times 7 = 8820$. As a comparison, a reference method (full system) would have had 185220 nonlinear unknowns. Figure 16 shows the response of the system for a traveling excitation. Both methods give identical results and show a reduction of the system amplitude.

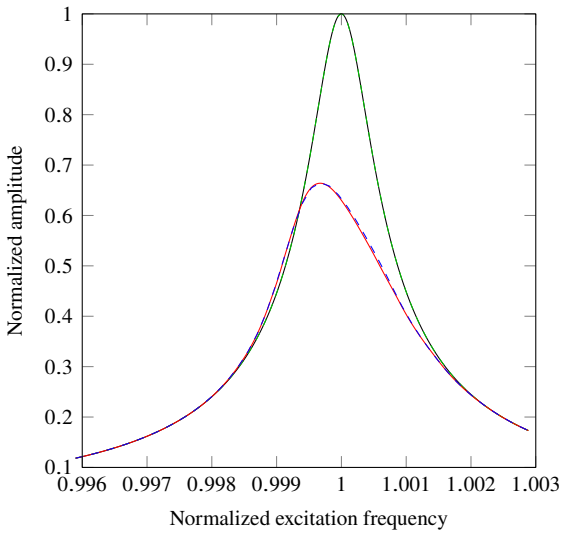

Figure 16. Frequency response function for a traveling wave excitation. (—)/(—): linear/nonlinear reference strategy and (- -)/(- -) linear/nonlinear new method.

Similarly, Figure 17 depicts the results for a standing wave and the solutions are in very good agreement.

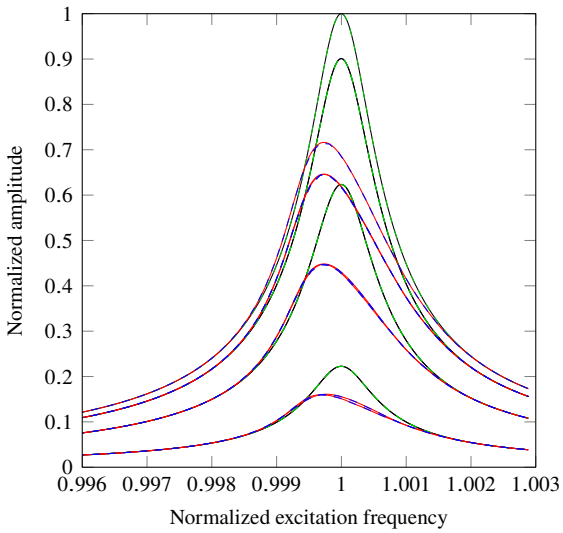

Figure 17. Frequency response function for a standing wave excitation. (—)/(—): linear/nonlinear reference strategy and (- -)/(- -) linear/nonlinear new method.

These results show the robustness of the proposed approach. Both methods took approximately the same computation time. However, the proposed approach gives the possibility to work immediately with the fundamental sector of the system without resorting to strategies which modify the mechanical system. The presented methodology is thus much easier to use, while offering the same level of accuracy.

6 Conclusion

This paper presents a cyclic symmetry theory applicable to structures with nonlinear cyclic boundary. A general framework is provided for any nonlinearity and method of resolution. Further derivations were provided for the case of a periodic and relative displacement, leading to a more reduced set of equations. This original approach has been validated on an academic and industrial shrouded blade systems. For the academic structure, the full system enacted as the reference whereas a technique of split shrouded turbine model was used as reference for the industrial case. Notice that the latter method is not always applicable and require strong modifications by the user, favoring the apparition of errors of the mechanical system. The proposed methodology solves all these issues. The approach allows the user to choose the cyclic expansion and can as such find standing wave solutions as well as localized one.

Acknowledgement

Samuel Quaegebeur is thankful for the financial support of the ANR (project ANR-22-CPJ2-0061-01).

References

[1] R. Valid and R. Ohayon. “Théorie et calcul statique et dynamique des structures à symétries cycliques”. La Recherche aérospatiale (1985), pp. 251–263.

[2] R. H. MacNeal. “NASTRAN cyclic symmetry capability. [application to solid rocket propellant grains and space antennas]”. 1973.

[3] D. L. Thomas. “Dynamics of rotationally periodic structures”. International Journal for Numerical Methods in Engineering Vol. 14, No. 1 (1979), pp. 81–102. DOI: 10.1002/nme.1620140107.

[4] E. P. Petrov. “A method for use of cyclic symmetry properties in analysis of nonlinear multiharmonic vibrations of bladed disks”. Journal of Turbomachinery Vol. 126, No. 1 (2004), p. 175. DOI: 10.1115/1.1644558.

[5] S. Quaegebeur, B. Chouvion, and F. Thouverez. "Model reduction of nonlinear cyclic structures based on their cyclic symmetric properties". Mechanical Systems and Signal Processing Vol. 145 (2020), p. 106970. DOI: 10.1016/j.ymssp.2020.106970.

[6] S.-T. Wei and C. Pierre. "Localization phenomena in mistuned assemblies with cyclic symmetry part I: free vibrations". Journal of Vibration, Acoustics, Stress, and Reliability in Design Vol. 110, No. 4 (1988), pp. 429–438. DOI: 10.1115/1.3269547.

[7] D.-M. Tran. "Component mode synthesis methods using partial interface modes: Application to tuned and mistuned structures with cyclic symmetry". Computers & Structures Vol. 87, No. 17 (2009), pp. 1141–1153. DOI: 10.1016/j.compstruc.2009.04.009.

[8] M. Krack, L. Panning-von Scheidt, J. Wallaschek, C. Siewert, and A. Hartung. "Reduced order modeling based on complex nonlinear modal analysis and its application to bladed disks with shroud contact". Journal of Engineering for Gas Turbines and Power Vol. 135, No. 10 (2013), pp. 102502–102502–8. DOI: 10.1115/1.4025002.

[9] G. Battiato. "Self-adaptive macroslip array for friction force prediction in contact interfaces with non-conforming meshes". Nonlinear Dynamics Vol. 106, No. 1 (2021), pp. 745–764. DOI: 10.1007/s11071-021-06888-0.

[10] X. Kan, K. Wang, and B. Zhao. "Dynamic characteristics of vibration localization of mistuned bladed disk due to shroud and blade damages". Journal of Low Frequency Noise, Vibration and Active Control (2023). Publisher: SAGE Publications Ltd STM, p. 14613484231209747. DOI: 10.1177/14613484231209747.

[11] R. Ahmed, C. M. Firrone, and S. Zucca. "A test rig for the full characterization of the dynamics of shrouded turbine blades". Mechanical Systems and Signal Processing Vol. 189 (2023), p. 110080. DOI: 10.1016/j.ymssp.2022.110080.

[12] C. Siewert, L. Panning, J. Wallaschek, and C. Richter. "Multiharmonic Forced Response Analysis of a Turbine Blading Coupled by Nonlinear Contact Forces". Journal of Engineering for Gas Turbines and Power Vol. 132, No. 8 (2010), pp. 082501–082501–9. DOI: 10.1115/1.4000266.

[13] F. Georgiades, M. Peeters, G. Kerschen, J. C. Golinval, and M. Ruzzene. "Modal analysis of a nonlinear periodic structure with cyclic symmetry". AIAA Journal Vol. 47, No. 4 (2009), pp. 1014–1025. DOI: 10.2514/1.40461.

[14] T. Heinze, L. Panning-von Scheidt, and J. Wallaschek. "Global detection of detached periodic solution branches of friction-damped mechanical systems". Nonlinear Dynamics Vol. 99, No. 3 (2020), pp. 1841–1870. DOI: 10.1007/s11071-019-05425-4.

[15] S. Quaegebeur, B. Chouvion, F. Thouverez, and L. Berthe. "Energy transfer between nodal diameters of cyclic symmetric structures exhibiting polynomial nonlinearities: Cyclic condition and analysis". Mechanical Systems and Signal Processing Vol. 139 (2020), p. 106604. DOI: 10.1016/j.ymssp.2019.106604.

[16] M. Krack and J. Gross. "Theory of harmonic balance". *Harmonic Balance for Nonlinear Vibration Problems*. Mathematical Engineering. Cham, 2019, pp. 11–46. DOI: 10.1007/978-3-030-14023-6_2.

[17] M. Mitra and B. I. Epureanu. "Dynamic modeling and projection-based reduction methods for bladed disks with nonlinear frictional and intermittent contact interfaces". Applied Mechanics Reviews Vol. 71, No. 5 (2019). Publisher: American Society of Mechanical Engineers Digital Collection. DOI: 10.1115/1.4043083.

[18] O. Poudou and C. Pierre. "Hybrid frequency-time domain methods for the analysis of complex structural systems with dry friction damping". *44th AIAA/ASME/ASCE/AHS/ASC Structures, Structural Dynamics, and Materials Conference*. DOI: 10.2514/6.2003-1411.

[19] T. M. Cameron and J. H. Griffin. "An alternating frequency/time domain method for calculating the steady-state response of nonlinear dynamic systems". Journal of Applied Mechanics Vol. 56, No. 1 (1989), pp. 149–154. DOI: 10.1115/1.3176036.

[20] D. D. Quinn. "A New Regularization of Coulomb Friction". Journal of Vibration and Acoustics Vol. 126, No. 3 (2004), pp. 391–397. DOI: 10.1115/1.1760564.

[21] M. Legrand and C. Pierre. “A compact, equality-based weighted residual formulation for periodic solutions of systems undergoing frictional occurrences”. 2023. hal-04189699.

[22] S. Nacivet, C. Pierre, F. Thouverez, and L. Jézéquel. “A dynamic Lagrangian frequency–time method for the vibration of dry-friction-damped systems”. Journal of Sound and Vibration Vol. 265, No. 1 (2003), pp. 201–219. DOI: 10.1016/S0022-460X(02)01447-5.

[23] M. Peeters, R. Viguié, G. Sérandour, G. Kerschen, and J. C. Golinval. “Nonlinear normal modes, Part II: Toward a practical computation using numerical continuation techniques”. Mechanical Systems and Signal Processing. Special Issue: Non-linear Structural Dynamics Vol. 23, No. 1 (2009), pp. 195–216. DOI: 10.1016/j.ymssp.2008.04.003.

[24] R. Seydel. Practical Bifurcation and Stability Analysis. 3rd ed. Interdisciplinary Applied Mathematics. New York, 2010.

[25] Y. Kuznetsov. Elements of Applied Bifurcation Theory. 3rd ed. Applied Mathematical Sciences. Springer-Verlag. New York, 2004. DOI: 10.1007/978-1-4757-3978-7.

[26] R. Craig and M. Bampton. “Coupling of substructures for dynamic analyses.” AIAA Journal Vol. 6, No. 7 (1968), pp. 1313–1319. DOI: 10.2514/3.4741.